



## FULL PAPER

# Design, synthesis, and in vitro biological evaluation of novel thiazolopyrimidine derivatives as antileishmanial compounds

Huseyin Istanbulu<sup>1</sup> | Gulsah Bayraktar<sup>2</sup> | Hasan Akbaba<sup>3</sup> | Ibrahim Cavus<sup>4</sup> | Gunes Coban<sup>2</sup> | Bilge Debelec Butuner<sup>3</sup> | Ali Ahmet Kilimcioglu<sup>4</sup> | Ahmet Ozbilgin<sup>4</sup> | Vildan Alptuzun<sup>2</sup> | Ercin Erciyas<sup>2</sup>

<sup>1</sup>Department of Pharmaceutical Chemistry, Faculty of Pharmacy, Izmir Katip Celebi University, Cigli, Izmir, Turkey

<sup>2</sup>Department of Pharmaceutical Chemistry, Faculty of Pharmacy, Ege University, Bornova, Izmir, Turkey

<sup>3</sup>Department of Pharmaceutical Biotechnology, Faculty of Pharmacy, Ege University, Bornova, Izmir, Turkey

<sup>4</sup>Department of Parasitology, Manisa Celal Bayar University, Manisa, Turkey

## Correspondence

Huseyin Istanbulu, Department of Pharmaceutical Chemistry, Faculty of Pharmacy, Izmir Katip Celebi University, 35620 Cigli, Izmir, Turkey.  
Email: [huseyin.istanbulu@ikc.edu.tr](mailto:huseyin.istanbulu@ikc.edu.tr)

## Funding information

Türkiye Bilimsel ve Teknolojik Arastirma Kurumu, Grant/Award Number: SBAG-213-S-026; Ege Üniversitesi, Grant/Award Number: 2014BIL003

## Abstract

A series of thiazolopyrimidine derivatives was designed and synthesized as a *Leishmania major* pteridine reductase 1 (*LmPTR1*) enzyme inhibitor. Their *LmPTR1* inhibitor activities were evaluated using the enzyme produced by *Escherichia coli* in a recombinant way. The antileishmanial activity of the selected compounds was tested in vitro against *Leishmania* sp. Additionally, the compounds were evaluated for cytotoxic activity against the murine macrophage cell line RAW 264.7. According to the results, four compounds displayed not only a potent in vitro antileishmanial activity against promastigote forms but also low cytotoxicity. Among them, compound **L16** exhibited an antileishmanial activity for both the promastigote and amastigote forms of *L. tropica*, with  $IC_{50}$  values of 7.5 and 2.69  $\mu$ M, respectively. In addition, molecular docking studies and molecular dynamics simulations were also carried out in this study. In light of these findings, the compounds provide a new potential scaffold for antileishmanial drug discovery.

## KEYWORDS

antileishmanial, *Leishmania major*, *Leishmania tropica*, neglected disease, PTR1 enzyme inhibition, thiazolo[5,4-*d*]pyrimidine

## 1 | INTRODUCTION

Leishmaniasis, one of the 20 neglected diseases classified by the WHO, is caused by a protozoa parasite from *Leishmania* species, which is transmitted to humans by the bite of the infected female phlebotomine sandflies. There are three main forms of the disease: visceral leishmaniasis (VL, Kala-azar), cutaneous leishmaniasis (CL), and mucocutaneous leishmaniasis (MCL).<sup>[1]</sup> Approximately one billion people are at the risk of this disease across the globe, and an estimated 0.7–1 million new cases of this disease and 26,000–65,000 deaths occur annually.<sup>[1,2]</sup>

More than 20 species of the unicellular protozoan parasites of the *Leishmania* genus can cause leishmaniasis in mammalian hosts. Among these, *Leishmania tropica* and *Leishmania major* are common causative agents for CL, whereas *Leishmania infantum* is a causative

agent for VL.<sup>[3]</sup> These parasites are also seen in Turkey, which is the bridge between Asia and Europe.<sup>[4]</sup>

The first-line drugs for the treatment of leishmaniasis are pentavalent antimonial compounds such as sodium stibogluconate (Pentostam™) and meglumine antimoniate (Glucantime™). Although, these drugs have been used since 1940s, their chemical structures were elucidated in the last two decades, but their mechanism of action has not been clarified yet.<sup>[5,6]</sup> However, it is known that these drugs are converted into an active form with the reduction from pentavalent to a trivalent form. The second-line drugs are amphotericin B (AmPB) and its liposomal form (AmBisome®), pentamidine, miltefosine, paromomycin, and some azoles (ketoconazole, itraconazole, and fluconazole).<sup>[7]</sup> Among these, miltefosine and azoles are the only options for oral treatment.

Regrettably, there are some limiting factors for using these drugs in the treatment of leishmaniasis: increasing drug resistance, high costs for AmBisome<sup>®</sup>, and severe adverse effects. For instance, it has been reported that resistance to miltefosine and antimonial drugs is up to 60% in India.<sup>[8-10]</sup> There are no data about resistance to these drugs in Turkey, but it is a fact that the war conditions in Syria and Iraq, and the advent of refugees in Turkey have increased the number of cases in Turkey.<sup>[11,12]</sup> Therefore, there is an urgent need for effective and safe chemotherapeutics against leishmaniasis.

Targeting the intracellular pathway is an important method for rational drug design and discovery. PTR1 is an NADPH-dependent, short-chained reductase enzyme family member, which can reduce a variety of unconjugated pteridines, as well as folates.<sup>[13,14]</sup> Folic acid and the related pteridines are essential cofactors for all life forms, especially for kinetoplastids. The active forms of both folate and biopterine are the reduced tetrahydro derivatives, which increase in *Leishmania* through the action of dihydrofolate reductase (DHFR) or the alternative pteridine reductase PTR1.<sup>[15]</sup> Unlike humans, kinetoplastids have a PTR1 enzyme. Therefore, the inhibition of the PTR1 enzyme appears to be a rational strategy for selective antileishmanial drug development.

The first information about the PTR1 enzyme (EC 1.5.1.33) was reported in 1992.<sup>[16,17]</sup> Later it was reported that this enzyme was an alternate source for the reduction of folate compounds and expressed PTR1 in transformed *Escherichia coli*.<sup>[13]</sup> Then, it was found that PTR1 was able to reduce folates to a minimal extent; its over-expression could compensate for the inhibition of DHFR by methotrexate (MTX).<sup>[18]</sup> The enzyme structure was reported by Hunter et al., and proteomic analyses for drug targets and resistance mechanisms were studied.<sup>[19,20]</sup>

According to a literature survey, the first reported PTR1 enzyme inhibitors are folate-like compounds bearing pteridine and quinoxaline ring as heterocyclic cores.<sup>[21]</sup> Among the six-membered fused rings, the structure-activity relationship of the substituted quinazoline core was examined extensively as PTR1 enzyme inhibitors with

antileishmanial activity.<sup>[22-24]</sup> On the contrary, bioisosteric replacement of pteridine and quinoxaline ring gave nonfolate inhibitors having benzothiazole, aminobenzimidazole, and pyrrolopyrimidine scaffolds. These nonfolate inhibitors showed good inhibition against the PTR1 enzyme at the micromolar level.<sup>[25-27]</sup>

The aims of this study are (a) to design and synthesize compounds bearing a thiazolopyrimidine ring, which is a bioisostere of the pteridine ring, (b) to test their PTR1 enzyme inhibitor activity, and (c) to investigate their antileishmanial and cytotoxic activities. In this study, thiazolopyrimidine scaffold was evaluated for antileishmanial activity for the first time.

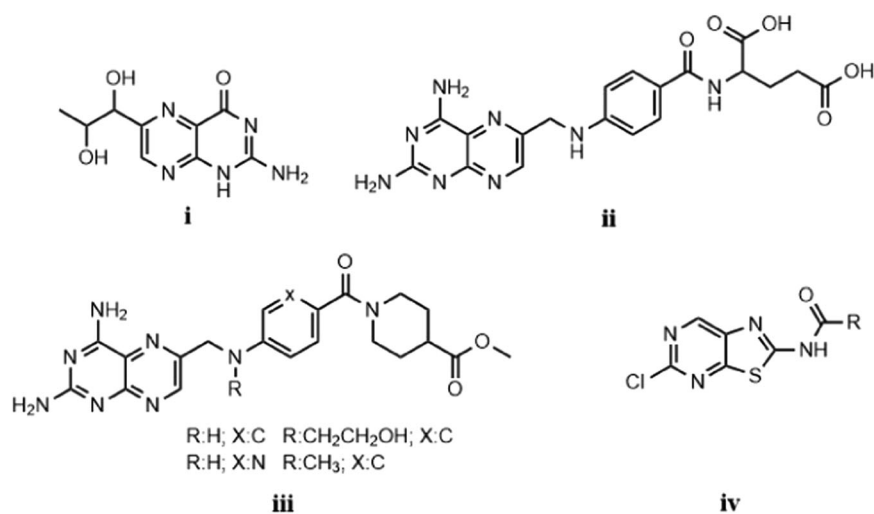
## 2 | RESULTS AND DISCUSSION

### 2.1 | Chemistry

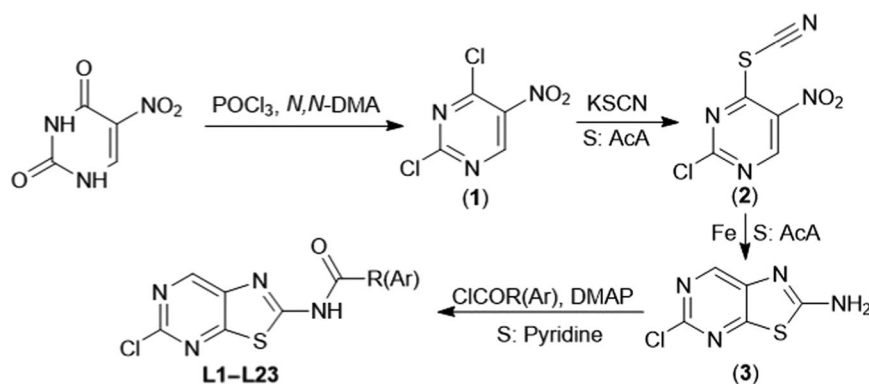
We designed novel compound derivatives from a 2-aminothiazolo[5,4-d]pyrimidine scaffold, which is an isostere of the pteridine ring (Figure 1). The compounds were derivatized by amidation of 2-amino function group with aliphatic and/or aromatic acyl groups.

All compounds were synthesized according to formerly published procedures in four steps (Scheme 1).<sup>[28-30]</sup> In the first step, 5-nitrouracil was converted to 2,4-dichloro-5-nitropyrimidine (**1**) by using phosphoryl chloride and *N,N*-dimethylaniline. Compound **1** was reacted with potassium thiocyanate to yield 2-chloro-4-thiocyanato-5-nitropyrimidine (**2**) in glacial acetic acid. Later, 2-amino-5-chlorothiazolo[5,4-d]pyrimidine (**3**) ring was obtained with the reduction of the nitro group using iron powder, followed by in situ cyclizations of compound **2**. In the last step, final amide derivatives, **L1-L23**, were obtained from compound **3** in the presence of 4-dimethylaminopyridine (DMAP) with various acyl chlorides in pyridine (Scheme 1).

The structures of the final compounds were determined by spectral analyses and the spectroscopic properties were in



**FIGURE 1** The chemical structures of biopterin (with pteridine ring structure), a substrate of PTR1 enzyme (i); antifolate compound aminopterin (ii); reported compounds with a PTR1 inhibitor activity (iii),<sup>[15]</sup> and synthesized compounds with thiazolopyrimidine ring, designed as bioisostere of the pteridine ring (iv)

**SCHEME 1** The synthesis pathway of compounds **L1–L23**

accordance with the proposed structures. According to the Fourier-transform infrared spectroscopy (FTIR) data, amide I and II bands were observed between  $1,724\text{--}1,686\text{ cm}^{-1}$  and  $1,572\text{--}1,585\text{ cm}^{-1}$  fields for aliphatic amides, whereas they were observed between  $1,660\text{--}1,698\text{ cm}^{-1}$  and  $1,575\text{--}1,584\text{ cm}^{-1}$  fields for aromatic amides. In the  $^1\text{H-NMR}$  (nuclear magnetic resonance) spectral data, compound **3** (2-amino-5-chlorothiazolo[5,4-*d*]pyrimidine) was identified with two proton signals: 8.49 ppm (singlet belonging to hydrogen on the aromatic ring) and 8.29 ppm (broad singlet of amino hydrogens). Unlike **L3**, the proton signal due to the amide NH group of **L1–L23** was recorded between 13.57 and 10.35 ppm as a broad singlet, and also the single proton signal of the heterocyclic ring was determined between 9.15 and 8.60 ppm as a singlet. In the spectrum, the shifts of these protons to the lower field supported the amide formation. On the contrary, in the case of compound **L21**, two doublets were observed at 6.93 and 7.81 ppm, with a 16-Hz coupling constant, which were assigned to the ethylenic protons that indicated *E* configuration. Some  $^1\text{H-NMR}$  spectra indicated the organic solvent impurities in the aliphatic region of the spectra, which were confirmed by the elemental analysis data as well.<sup>[31,32]</sup> The obtained elemental analysis data of the compounds were within 0.4% impurity of the predicted structures. In addition, observed carbon signals in the  $^{13}\text{C-NMR}$  of the compounds were in accordance with the molecular structures; however, some compounds were not subjected to  $^{13}\text{C-NMR}$  analysis due to solubility issues. According to electrospray ionization–mass spectroscopy (ESI–MS) data, molecular ion peaks, isotope peaks, and fragmentation patterns were determined as expected.

The characterization data of all compounds are reported in the experimental section in detail, and all compounds, except **L1**, are reported for the first time in this study. The spectral data of **L1** were in accordance with the formerly reported literature.<sup>[28]</sup>

## 2.2 | Biological activities

### 2.2.1 | LmPTR1 enzyme expression and in vitro inhibition assay

*In vitro* enzyme inhibition studies were performed according to the literature with slight modifications, as explained in Section 4.<sup>[21]</sup>

MTX was used as the reference compound.  $\text{IC}_{50}$  values of the title compounds are listed in Table 1.

According to activity results, most of the compounds bearing amide group displayed a better enzyme inhibitor activity than compound **3**, with an amine group at 2-position of 5-chlorothiazolo[5,4-*d*]pyrimidine. Among the studied compounds, the compound bearing acetyl moiety (**L1**) displayed the best inhibitor potency with the  $\text{IC}_{50}$  value of  $43.8 \pm 1.9\ \mu\text{M}$ . In general, the replacement of the acetyl group with the other aliphatic acyl groups such as propanoyl (**L2**,  $\text{IC}_{50}$   $75.5 \pm 1.7\ \mu\text{M}$ ), butanoyl (**L3**,  $\text{IC}_{50}$   $52.6 \pm 1.4\ \mu\text{M}$ ), and isobutanoyl (**L4**,  $\text{IC}_{50}$   $81.1 \pm 2.5\ \mu\text{M}$ ) did not improve the inhibitory activity against *LmPTR1*.

When benzoyl derivatives were evaluated within themselves, it was observed that the introduction of a substituent to the phenyl ring resulted in an increased inhibitor activity, except for fluorine substituent.

Generally, the results showed that the conversion of the amine groups on 5-chlorothiazolo[5,4-*d*]pyrimidine ring to amide function by attaching an aliphatic or an aromatic moiety affected the enzyme inhibitory activity positively.

### 2.2.2 | In vitro antileishmanial activity

Targeting the folate pathway by inhibiting the PTR1 enzyme, which is a bypass of DHFR inhibition in the parasites' folate pathway, is a feasible strategy for selective antileishmanial chemotherapy.<sup>[33]</sup>

As *LmPTR1* enzyme inhibition is one of the possible targets to combat leishmaniasis, the compounds were tested for their *in vitro* antileishmanial activity. For antileishmanial activity, the percentage viability of parasites was studied against *L. tropica*, *L. infantum*, and *L. major* at 24, 48, and 72 hr, respectively. As the observed percentage viabilities were similar in terms of time and parasite species,  $\text{IC}_{50}$  values were calculated for 24 hr in *L. tropica* promastigote (Table 1). **L19** was found to be the most active one with the  $\text{IC}_{50}$  value of  $0.5 \pm 0.4\ \mu\text{M}$ , followed by **L16** with the  $\text{IC}_{50}$  value of  $7.5 \pm 4.6\ \mu\text{M}$ . Among the phenyl derivatives, generally, the introduction of a substituent to *para* position resulted in a remarkable improvement in the antileishmanial activity, whereas *ortho* substitution led to a lack of activity. This result was noticeably observed in chlorine substitution.

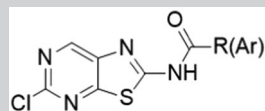


**TABLE 1** Synthesized compounds and their *LmPTR1* enzyme inhibitor activity and in vitro antileishmanial activity against *Leishmania tropica* (*L. tropica*) promastigote

	R (Ar)	<i>LmPTR1</i> IC <sub>50</sub> ( $\mu\text{M} \pm \text{SD}$ )	<i>L. tropica</i> IC <sub>50</sub> ( $\mu\text{M} \pm \text{SD}$ )
L1	methyl	43.8 $\pm$ 1.9	>100
L2	ethyl	75.5 $\pm$ 1.7	>100
L3	propyl	52.6 $\pm$ 1.4	67.7 $\pm$ 7.9
L4	isopropyl	81.1 $\pm$ 2.5	>100
L5	cyclohexane	62.8 $\pm$ 2.4	27.3 $\pm$ 2.8
L6	phenyl	86.5 $\pm$ 2.0	>100
L7	2-methylphenyl	52.4 $\pm$ 2.1	>100
L8	2-methoxyphenyl	72.1 $\pm$ 2.3	>100
L9	2-chlorophenyl	69.1 $\pm$ 2.6	>100
L10	2-fluorophenyl	>100	>100
L11	2-bromophenyl	73.8 $\pm$ 2.4	>100
L12	2-iodophenyl	nd <sup>a</sup>	>100
L13	2-trifluoromethyl phenyl	nd <sup>a</sup>	>100
L14	4-methylphenyl	76.5 $\pm$ 1.8	>100
L15	4-methoxyphenyl	nd <sup>a</sup>	37.1 $\pm$ 21.0
L16	4-chlorophenyl	74.8 $\pm$ 1.2	7.5 $\pm$ 4.6
L17	4-fluorophenyl	>100	61.0 $\pm$ 13.1
L18	4-nitrophenyl	77.2 $\pm$ 2.8	10.1 $\pm$ 6.2
L19	2,4-dichlorophenyl	nd <sup>a</sup>	0.5 $\pm$ 0.4
L20	2-phenylethyl	>100	22.5 $\pm$ 3.3
L21	styryl	nd <sup>a</sup>	8.4 $\pm$ 2.8
L22	2-furyl	>100	>100
L23	2-thienyl	nd <sup>a</sup>	>100
3	-	97.1 $\pm$ 2.6	>100
Methotrexate	-	6.3 $\pm$ 0.5	-
Amphotericin B <sup>®</sup>			0.2 $\pm$ 0.02
Glucantime <sup>®</sup>			5.8 $\pm$ 1.4

Abbreviation: SD, standard deviation.

<sup>a</sup>The activity of the compound was non-detectable due to solubility problems.

Interestingly, the addition of 2-chlorine substitution to 4-chlorine derivative improved the activity significantly. On the contrary, the derivative bearing phenylethyl group showed up to a four-fold better activity, compared with ethyl-chained aliphatic amide; therefore, the substitution of ethyl with phenyl group improved the activity. Additionally, styryl derivative was found to be nearly three-fold more active than its saturated analog, phenylethyl derivative.

On the basis of antileishmanial activity results against *L. tropica* promastigote, **L16** and **L19** were selected for the further amastigote

assay. The results were expressed in the means of percent decrease as compared with the positive control. Infection percentages were calculated by the multiplication of infected macrophage percent with an average number of amastigotes per infected macrophage.<sup>[34]</sup> IC<sub>50</sub> values of **L16** and **L19** were found to be 2.69  $\mu\text{M}$  (0.07–9.17) and 185.4  $\mu\text{M}$  (97.22–418.2), respectively (Table 2 and Figure S15). Negative control amphotericin B gave an IC<sub>50</sub> value of 0.065  $\mu\text{M}$  (0.04–0.1).

Taken together, **L16** has an antileishmanial potential for both promastigotes and amastigotes.

**TABLE 2** The antileishmanial activity of the selected compounds against *L. tropica* amastigotes

Compound	IC <sub>50</sub> (μM)
L16	2.69 (0.07–9.17)
L19	185.4 (97.22–418.2)
Amphotericin B	0.065 (0.04–0.1)

Note: The bottom and top values are given in brackets.

### 2.2.3 | Cytotoxicity assay

The cytotoxicity assay was performed against RAW 264.7 murine macrophage cell line for the compounds which showed the best in vitro antileishmanial activity.<sup>[35,36]</sup> The compounds showed low (L18, L19) or no (L16, L21) cytotoxicity (Table 3). Therefore, these results indicate that the title compounds exhibit selective toxicity.

### 2.3 | Molecular modeling studies

In the current study, molecular docking was carried out to detect binding orientations and affinity of thiazolopyrimidine derivatives in the active site of *LmPTR1* (PDB id: 2BFA resolved at 2.7 Å) using Gold 5.2.1 program. Docking scores of the first-ranked docking solutions of the studied compounds are reported in Table 4. Before the docking study, 10-propargyl-5,8-dideazafoolic acid (CB3717) taken from the crystal structure of *LmPTR1* (PDB id: 2BFA) was docked in *LmPTR1* to validate the docking method.

The first-ranked docking pose and the scoring value of CB3717 inside the *LmPTR1* are figured in Figure S1 and reported in Table 4. It was observed that the quinazoline ring of CB3717 obtained from the docking study was settled into the pteridine-binding pocket of *LmPTR1*, similar to the ternary complex of *LmPTR1* (PDB id: 2BFA; Figure S1). The minor difference between the docking pose and the crystal form of CB3717 is the orientation of the glutamate tail of the inhibitor compound. Although the glutamate tail obtained from the docking pose extended Gln186 and Leu189, the tail of the crystal form oriented toward the opposite side. The comparison of the first-ranked solutions and crystal form of CB3717 inside *LmPTR1* is given in Figure S1.

In consideration of enzyme inhibition assay, L1 displayed the best inhibitory activity against *LmPTR1* among the studied compounds. According to docking study results, the first-ranked docking pose of L1 partially occupied the catalytic center of *LmPTR1* (Figure S2). It was observed that the acetamide group of the L1 was placed between Ser111, Ser112, Phe113, and the phosphate and ribose fragment of the cofactor; while the thiazolopyrimidine ring of the L1 was sandwiched between Phe113 and nicotinamide group of the cofactor. The other selected compounds, L9 and L18, were placed in the catalytic site of *LmPTR1*, formed by amino acid residues Ser111, Phe113, Asp181, Tyr194, and Lys198, and nicotinamide and ribose component of the cofactor. It was observed that while the

**TABLE 3** Selected compounds' in vitro cytotoxic activity against RAW 264.7 murine macrophage cell line

Compound	In vitro cytotoxicity IC <sub>50</sub> (μM ± SD) RAW 264.7
L16	>100
L18	77.1 ± 0.14
L19	82.9 ± 1.02
L21	>100
Pentostam®	>100

Abbreviation: SD, standard deviation.

thiazolopyrimidine ring of these compounds was shifting toward Ser111 and the phosphate and ribose components of the cofactor, the titled ring was sandwiched between Phe113 and nicotinamide component of NADPH as the quinazoline ring of CB3717 in the crystal form of the ternary complex.

In addition, the occupancy of the substituted benzamide groups of L9 and L18 in the catalytic site was similar to *p*-aminobenzamide group of CB3717 in the catalytic site of *LmPTR1* (Figures S1, S5, and S11). L16, the other selected compound, occupied the catalytic site of *LmPTR1* by an opposite orientation as compared with orientations of L9 and L18 inside *LmPTR1*. It was detected that, when substituted benzamide group of L16 settled between Phe113 and nicotinamide component of the cofactor, thiazolopyrimidine ring shifted to be placed between Leu188, Tyr191, Tyr194, and Lys198 (Figure S8). The comparison of the first-ranked solutions of the studied compounds in *LmPTR1* is given in Figure 2.

**TABLE 4** Docking scores for thiazolopyrimidine derivatives in the active site of *LmPTR1* (PDB id: 2BFA) using Goldscore

Compounds	<i>LmPTR1</i> (2BFA) Goldscore	Compounds	<i>LmPTR1</i> (2BFA) Goldscore
L1	51.5110 (1)	L14	64.3328 (1)
L2	53.3057 (1)	L15	65.9658 (1)
L3	56.9219 (1)	L16	64.7663 (1)
L4	56.0127 (1)	L17	62.5242 (1)
L5	62.5664 (1)	L18	64.7168 (1)
L6	61.8942 (1)	L19	66.4583 (1)
L7	64.1272 (1)	L20	62.5019 (1)
L8	64.8221 (1)	L21	70.2491 (1)
L9	64.2589 (1)	L22	58.7457 (1)
L10	61.0443 (1)	L23	63.0418 (1)
L11	65.3434 (1)	3	45.7886 (1)
L12	66.8230 (1)	Methotrexate	76.8028 (1)
L13	64.0401 (1)	CB3717	75.1539 (1)

Note: The absolute ranking positions for the suggested binding poses are given inside brackets.

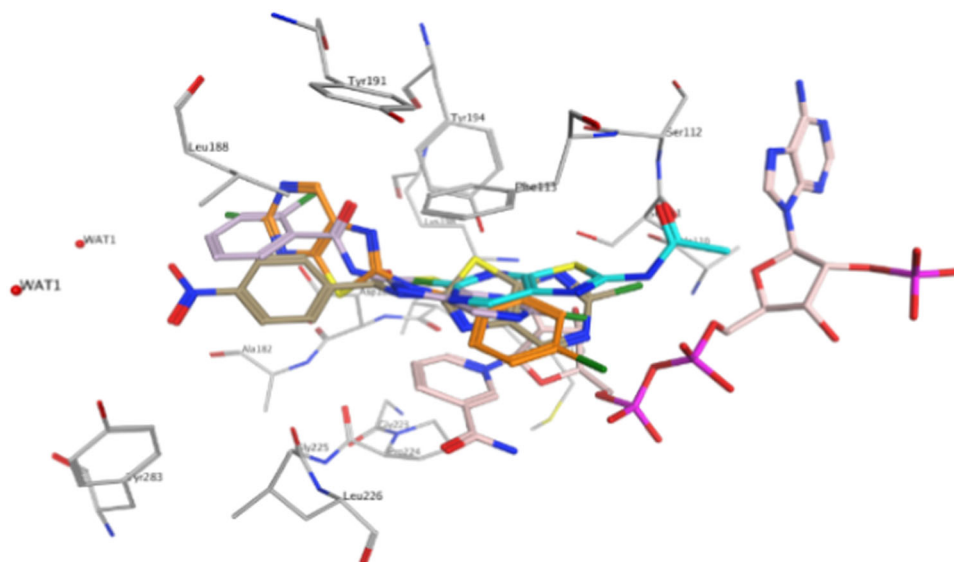


**FIGURE 2** The comparison of the first-ranked solutions of the studied compounds in *LmPTR1* (PDB id: 2BFA). Cyan, light purple, orange, and army green sticks represent compounds **L1**, **L9**, **L16**, and **L18**, respectively. The active site residues are named and represented as gray sticks in *LmPTR1*. For a clear image, all hydrogen atoms were hidden

In our study, the molecular dynamics (MD) simulations and MM-GBSA binding free energy calculations were executed to analyze noncovalent interactions of thiazolopyrimidine derivatives, namely compounds **L1**, **L9**, **L16**, and **L18**, in the active site of *LmPTR1*. For this purpose, the first-ranked solutions of compounds **L1**, **L9**, **L16**, and **L18**, yielded by using the GOLD 5.2.1 program, were chosen for MD simulations. The protein-ligand-cofactor ternary complexes of the selected compounds were then subjected to 100-ns simulations after the equilibrium step.

The analysis of the stability of ternary complexes of the selected compounds revealed that the MD simulations for the stability of these complexes were observed to be stable during the whole MD simulation. The average root mean square deviation (RMSD) value of the ternary complex of **L1** was detected, which fluctuated between  $\sim 1.5$  Å and  $\sim 2.5$  Å throughout the whole simulation. Moreover, the average RMSD value of **L1** was determined, revealing that it preserved its stability,  $\sim 0.5$  Å, from beginning to end of MD simulation (Figure S3). It was displayed that **L1** kept its position in the active site of *LmPTR1*, preserving key interactions with protein and cofactor (Figure S4). The RMSD value of the ternary complex of **L9** was found to be increased, fluctuating from  $\sim 1.5$  Å to  $\sim 2.0$  Å at the first 20 ns of MD simulations. Later, its fluctuations increased to  $\sim 2.5$  Å, and it fluctuated between  $\sim 2.0$  and  $\sim 3.0$  Å at rest of the MD simulations. A similar fluctuation behavior was observed for the RMSD plot of the ternary complex of **L18** in its MD simulations. The RMSD value of the ternary complex was found to be increased, fluctuating from  $\sim 1.5$  to  $\sim 2.5$  Å at the first 20 ns of MD simulations, and after this increase, it fluctuated between  $\sim 2.0$  and  $\sim 3.0$  Å at rest of the MD simulations. The average RMSD value of **L9** was stable,  $\sim 0.5$  Å, in the entire MD simulation (Figure S6), similar to the RMSD value of **L1**. Therefore, no change was observed at the position of **L9** in the active site of

*LmPTR1* (Figure S7). About the average RMSD value of the **L18**, periodical changes were viewed between  $\sim 0.5$  and  $\sim 1.0$  Å and this was observed when the substituted benzamide group of **L18** was rotating, ligand kept its orientation and location (Figures S12 and S13). There was a gradual increase in the average RMSD value of the ternary complex of **L16**,  $\sim 1.5$  to  $\sim 3.5$  Å, throughout 75 ns of MD simulations, and then it decreased to  $\sim 2.5$  Å during the rest of MD simulation. As the RMSD value of **L16** was evaluated, it was observed that there were periodically changing fluctuations between  $\sim 0.5$  and  $\sim 1.0$  Å in the entire simulation (Figure S9). It was monitored that **L16** returned starting binding orientations, however, it was located different regions of the active site of *LmPTR1* during the MD simulations (Figure S10).

In the MD plots of the binary complex formed by NADPH and *LmPTR1*, the average RMSD value fluctuated between  $\sim 1.5$  and  $\sim 2.2$  Å throughout the whole MD simulation (Figure S14).

The binding mode analysis revealed that several noncovalent interactions were observed between the studied compounds and NADPH-*LmPTR1* complexes such as hydrogen bonding, cation- $\pi$ , and  $\pi$ - $\pi$  interactions. It was observed that major efficiencies of the titled interactions were different for the binding mode of the studied compounds. According to analysis results, hydrogen bonding formed by a direct bonding with Tyr194, cofactor, and water molecules, and water-mediated bonding with backbone residues and cofactor is the major factor for binding of **L1** inside the active site of *LmPTR1* (Tables S1-S3). Besides hydrogen-bonding network,  $\pi$ - $\pi$  interactions formed by the nicotinamide group of the cofactor, Phe113, and thiazolopyrimidine ring of **L1** as sandwich-type  $\pi$ - $\pi$  stacking contributed to the bonding of the title compound (Figure S4). The main interaction contributing to the binding mode of **L9** and **L18** is a sandwich-type  $\pi$ - $\pi$  interaction formed by

Phe113, the nicotinamide group of the cofactor, and the thiazolopyrimidine ring of the studied compounds (Figures S7 and S13). Hydrogen bonding, formed by water molecules and water-mediated bonding with backbone residues and cofactor, is the secondary interaction that contributes to the formation of the binding mode of **L9** and **L18** inside *LmPTR1*. For these two molecules, direct hydrogen bonding with backbone residues and cofactor was observed with low frequencies during the whole MD simulation (Tables S4–S6 and S10–S12). Lastly, in the binding mode analysis of **L16**, two main interactions, which contribute to the binding process inside *LmPTR1*, were observed as hydrogen bonding and cation- $\pi$  interactions between thiazolopyrimidine ring and the positively charged guanidine group of Arg284 (Figure S10 and Tables S7–S9). For all studied compounds, hydrogen bond formed between related heteroatoms of the compounds and the hydroxyl group of ribose ring of cofactor with several hydrogen-bonding frequencies was detected (Tables S1, S4, S7, and S10).

The MM-GBSA binding free energy calculations and energy decomposition analysis were performed for compounds **L1**, **L9**, **L16**, and **L18** from free MD simulations. The average binding free energies of the title compounds inside the active site of *LmPTR1* are tabulated in Table 5, and the results of energy decomposition analysis are tabulated in Tables S13–16.

The average binding free energies of the studied compounds were calculated around  $-20$  kcal/mol, and no significant difference was observed among the compounds. At the same time, the experimental binding energies of the studied compounds were calculated between  $-5.5$  and  $-6.0$  kcal/mol (Table 5). According to binding free energy calculations, the unfavorable contribution is provided from the electrostatic energies (in vacuum and solvent) for both systems. Besides, the van der Waals energies and nonpolar solvation energies are the important factors in contrast to the electrostatic (in vacuum) and polar solvation energies (in solvent) for the binding of the title compounds to the active site of *LmPTR1* (Table 5). Polar solvation energies, obtained from MD

simulations of the title compounds, confirm that the hydrogen bond was formed by water molecules. The electrostatic energies (in vacuum) only contribute to the binding free energy of **L1** and **L16**. The energy decomposition analysis of **L1** revealed that Phe113, Met183, Tyr19,4, and NADPH provide important energy contributions in a ternary complex system (Table S13). The van der Waals and nonpolar solvation energies are dominant components for the binding of the ligand, which are supplied by Phe113 and NADPH; therefore, this shows the contribution of Phe113 and NADPH to form a  $\pi$ - $\pi$  interaction with ligand in the active site of *LmPTR1*. For **L9**, the van der Waals and nonpolar solvation energies are the main factors for the contribution of the binding free energy provided by Phe113, Leu188, Tyr194, and cofactor. In addition to this, polar solvation energy provided by NADPH contributes to binding free energy as well as the van der Waals and nonpolar solvation energies (Table S14). The van der Waals and nonpolar solvation energies provided by Phe113 and NADPH support the sandwich  $\pi$ - $\pi$  interaction between thiazolopyrimidine ring and titled residues. The energy decomposition analysis of **L16** revealed that the van der Waals and nonpolar solvation energies play a crucial role in the binding process in the ligand-NADPH-*LmPTR1* ternary complex. The calculated van der Waals and nonpolar solvation energies display the contribution of hydrophobic interactions for the binding process (Table S15). Also, the contribution of electrostatic energy supplied by Arg284 supports the formation of cation- $\pi$  interaction between the positively charged guanidine group of Arg284 and thiazolopyrimidine ring of the **L16** (Table S15). The energy decomposition analysis of **L18** revealed that the van der Waals and nonpolar solvation energies are the largest contributions to binding free energy (Table S16). Especially, the favorable contributions for binding free energy are the van der Waals and nonpolar solvation energies provided by NADPH and Phe113, interacting with **L18** for the binding process. These contributions support the binding mode of **L18**, similar to the binding mode of compound **L9** that is sandwiched between Phe113, cofactor, and ligand.

**TABLE 5** The calculated MM-GBSA (Molecular Mechanics - Generalized Born Surface Area) binding free energies (delta total energy) and their components for compounds **L1**, **L9**, **L16**, and **L18** inside *LmPTR1* with standard errors of the mean

	<b>L1</b>	<b>L9</b>	<b>L16</b>	<b>L18</b>
van der Waals energy (kcal/mol)	$-27.0527 \pm 0.0396$	$-35.6598 \pm 0.0406$	$-32.4403 \pm 0.0498$	$-37.6610 \pm 0.0584$
Electrostatic energy (kcal/mol)	$-14.4281 \pm 0.0923$	$2.2817 \pm 0.0682$	$-15.2893 \pm 0.0821$	$0.3036 \pm 0.0604$
Polar solvation energy (kcal/mol)	$25.4838 \pm 0.049$	$16.4761 \pm 0.0681$	$29.7441 \pm 0.0656$	$18.1820 \pm 0.0572$
Nonpolar solvation energy (kcal/mol)	$-3.2060 \pm 0.0051$	$-3.3994 \pm 0.0049$	$-3.9665 \pm 0.0043$	$-3.8218 \pm 0.0066$
Delta gas-phase free energy (kcal/mol)	$-41.4808 \pm 0.0979$	$-33.3781 \pm 0.0947$	$-47.7296 \pm 0.0877$	$-37.3574 \pm 0.0935$
Delta solvation free energy (kcal/mol)	$22.2778 \pm 0.0624$	$13.0767 \pm 0.0650$	$25.7776 \pm 0.0633$	$14.3602 \pm 0.0545$
Delta total energy (kcal/mol)	$-19.2031 \pm 0.0489$	$-20.3014 \pm 0.0417$	$-21.9519 \pm 0.0425$	$-22.9972 \pm 0.0590$
IC <sub>50</sub> ( $\mu$ M)	$43.8 \pm 1.9$	$69.1 \pm 2.6$	$74.8 \pm 1.2$	$77.2 \pm 2.8$
Experimental binding energy (kcal/mol)	$-5.9824^a$	$-5.7106^a$	$-5.6634^a$	$-5.6445^a$

<sup>a</sup>Experimental binding free energy was calculated from IC<sub>50</sub> values according to  $\Delta G \approx RT \ln IC_{50}$ .

### 3 | CONCLUSION

In this study, a series of thiazolopyrimidine derivatives was designed and synthesized as antileishmanial compounds with *LmPTR1* inhibitor activity. Regarding the activity results, the conversion of the amine group to the amide function on the main ring affects the enzyme inhibitory activity. Among them, the 2,4-dichlorobenzoyl derivative (**L19**) was found to be the most active compound. First, the antileishmanial activity of the compounds against promastigote form was evaluated, and then the most promising ones were tested against amastigote forms of the parasite. It was found out that **L16** was quite active for both promastigote and amastigote forms of the parasite, whereas **L19** showed remarkable activity against the promastigote form of the parasite. Moreover, selected derivatives displayed low cytotoxicity. Interestingly, there is no correlation between enzyme inhibitory activity and antileishmanial activity. Taken together, it might be speculated that the antileishmanial activity occurs via different mechanisms.

MD simulations, guided by docking studies, of compounds **L1**, **L9**, **L16**, and **L18** inside *LmPTR1* showed that hydrogen-bonding networks played a key role in the stability of the title compounds in the active site of *LmPTR1*. Especially, the formation of hydrogen bonds with backbone residues for **L1** was observed more frequently, compared with the other studied compounds. It was determined that hydrogen bonding formed by water molecules and water-mediated bridges contributed to the binding process of all studied compounds inside *LmPTR1*. In addition to hydrogen bonding, it was detected that the cation- $\pi$  interaction was the secondary dominant factor for the binding process of the **L16**, and  $\pi$ - $\pi$  interaction was the secondary dominant factor for the binding process of **L9** and **L18** inside *LmPTR1*. According to enzyme inhibition assay, **L1** has a slightly higher inhibitory activity against *LmPTR1*, compared with the other studied compounds, and considering the molecular modeling studies, it might be concluded that hydrogen bonds formed especially with Tyr194 caused this difference.

## 4 | EXPERIMENTAL

### 4.1 | Chemistry

#### 4.1.1 | General

Most of the reagents and solvents were commercially available materials of reagent grade and were purchased from Alfa Aesar, TCI Chemicals, Sigma-Aldrich, or Merck. Melting points were determined with the capillary melting point apparatus (Barnstead Electrothermal IA 900). Analytical thin-layer chromatography was run on Merck silica gel plates (Kieselgel 60 F254) with detection by ultraviolet light (254 nm). The FTIR spectra of the compounds were monitored by attenuated total reflectance (PerkinElmer Spectrum 100 FT-IR, Shelton). The NMR spectra (400 MHz for  $^1\text{H}$ -NMR and 100 MHz for  $^{13}\text{C}$ -NMR) were recorded in the deuterated solvent on AS400

Mercury Plus NMR Varian (Varian Inc., Palo Alto, CA). Chemical shifts were measured in parts per million ( $\delta$ ). Coupling constants ( $J$ ) were reported in hertz (Hz). Liquid chromatography-mass spectrometry (MS) was recorded on a Thermo MSQ Plus/DSQ II (San Jose, CA) mass spectrometer using the ESI<sup>+</sup> method. Elemental analyses were performed on Leco TruSpec Micro CHNS (Leco, St. Joseph, MI), and the values were found to be within  $\pm 0.4\%$  of the theoretical values.

The InChI codes of the investigated compounds, together with some biological activity data, are provided as Supporting Information.

#### 4.1.2 | Synthesis of the title compounds

2-Amino-5-chlorothiazolo[5,4-*d*]pyrimidine derivatives were prepared in four steps according to the procedure in the literature (Scheme 1).<sup>[28-30]</sup> In the first step, 7.3 ml of freshly distilled POCl<sub>3</sub> (0.08 mol) was carefully added to the mixture of 5-nitrouracil (3.14 g, 0.028 mol) and *N,N*-dimethylaniline (3.54 ml, 0.028 mol) in an ice bath for 30 min. The reaction mixture was stirred at 60°C for 5.5 hr. After cooling to room temperature, the mixture was poured into 100 ml of ice water. The solution was extracted with diethyl ether (3  $\times$  100 ml). The organic layer was washed with brine, dried over anhydrous Na<sub>2</sub>SO<sub>4</sub>, and concentrated in vacuo to obtain 2,4-dichloro-5-nitrouracil (compound **1**). Compound **1** was used without further purification.

Compound **1** (1.91 g, 0.01 mol) was added to 5-ml glacial acetic acid and cooled down to 0°C using an ice bath. Potassium thiocyanate (1.07 g, 0.0111 mol) was added in portions over 30 min and the mixture was stirred at 0°C for 2 hr. The reaction mixture was poured into crushed ice, filtered, and washed with cold diethyl ether to give 2-chloro-5-nitro-4-thiocyanatopyrimidine (compound **2**). The crude product was used without further purification for the next step.

In the third step, the mixture of compound **2** (2 g, 9.23 mmol) and iron powder (1.55 g, 27.7 mmol) in glacial acetic acid (18.5 ml) was refluxed for 2 hr. The reaction mixture was cooled to room temperature and filtrated. The filtrate was evaporated under reduced pressure. The residue was diluted with water and then extracted with ethyl acetate (3  $\times$  50 ml). The combined organic layer was washed with saturated NaHCO<sub>3</sub> solution and saturated NH<sub>4</sub>Cl solution, dried over anhydrous Na<sub>2</sub>SO<sub>4</sub>, and evaporated under vacuum. The crude product was crystallized from ethanol to yield 2-amino-5-chlorothiazolo[5,4-*d*]pyrimidine ring (compound **3**).

The final compounds, **L1-L23**, were obtained from compound **3** with various acyl chlorides. Compound **3** (0.3 g, 1.6 mmol) in pyridine was treated with acyl chlorides (3.2 mmol) in an ice bath. DMAP was added to the reaction mixture in a catalytic amount, and it was stirred at room temperature overnight. The pH of the reaction medium was adjusted to  $\sim 2$  with 2-N HCl solution, and then it was extracted with ethyl acetate (3  $\times$  50 ml). After the combined organic extracts were washed with saturated NaHCO<sub>3</sub> solution, dried over anhydrous Na<sub>2</sub>SO<sub>4</sub>, and evaporated under reduced pressure, the final

compounds were crystallized from ethanol, methanol, ethyl acetate, or tetrahydrofuran.

#### N-(5-Chlorothiazolo[5,4-d]pyrimidin-2-yl)acetamide (L1)<sup>[28]</sup>

Yield 71% (yellow solid). mp. 205°C. FTIR  $\nu_{\max}$   $\text{cm}^{-1}$ : 1,724 and 1,584. <sup>1</sup>H-NMR (dimethyl sulfoxide DMSO-*d*<sub>6</sub>, 400 MHz)  $\delta$ : 2.21 (s, 3H), 9.05 (s, 1H), and 12.78 (br, 1H). <sup>13</sup>C-NMR (DMSO-*d*<sub>6</sub>, 100 MHz)  $\delta$ : 23.1, 140.4, 149.7, 153.4, 158.9, 166.0, and 170.7. MS (ESI<sup>+</sup>): *m/z*: 229.1 [M+H]<sup>+</sup> and 231.1 [M+2+H]<sup>+</sup>. Anal. (C<sub>7</sub>H<sub>5</sub>ClN<sub>4</sub>OS.0.5H<sub>2</sub>O.0.33CH<sub>3</sub>OH) calcd: C 35.47, H 2.97, N 22.57, S 12.92; found: C 35.85, H 3.36, N 22.55, S 12.59.

#### N-(5-Chlorothiazolo[5,4-d]pyrimidin-2-yl)propionamide (L2)

Yield 73% (yellow solid). mp. 241°C. FTIR  $\nu_{\max}$   $\text{cm}^{-1}$ : 1,692 and 1,572. <sup>1</sup>H-NMR (DMSO-*d*<sub>6</sub>, 400 MHz)  $\delta$ : 1.10 (t, 3H, *t*, *J* = 7.6 Hz), 2.54 (q, 2H, *J* = 7.6 Hz), 9.07 (s, 1H), and 12.75 (br, 1H). <sup>13</sup>C-NMR (DMSO-*d*<sub>6</sub>, 100 MHz)  $\delta$ : 9.1, 28.9, 140.3, 149.7, 153.2, 158.8, 165.9, and 174.4. MS (ESI<sup>+</sup>): *m/z*: 243.2 [M+H]<sup>+</sup> and 245.2 [M+2+H]<sup>+</sup>. Anal. (C<sub>8</sub>H<sub>7</sub>ClN<sub>4</sub>OS) calcd: C 39.59, H 2.91, N 23.09, S 13.21; found: C 39.77, H 3.10, N 23.47, S 13.45.

#### N-(5-Chlorothiazolo[5,4-d]pyrimidin-2-yl)butyramide (L3)

Yield 72% (beige solid). mp. 194°C. FTIR  $\nu_{\max}$   $\text{cm}^{-1}$ : 1,709 and 1,585. <sup>1</sup>H-NMR (DMSO-*d*<sub>6</sub>, 400 MHz)  $\delta$ : 0.91 (t, 3H, *J* = 7.6 Hz), 1.63 (m, 2H, *J* = 7.2 Hz), 2.48 (br, 2H), 9.04 (s, 1H), and 12.77 (br, 1H). <sup>13</sup>C-NMR (DMSO-*d*<sub>6</sub>, 100 MHz)  $\delta$ : 13.9, 18.2, 37.4, 140.3, 149.8, 153.2, 158.8, 165.8, and 173.6. MS (ESI<sup>+</sup>): *m/z*: 257.0 [M+H]<sup>+</sup> and 259.1 [M+2+H]<sup>+</sup>. Anal. (C<sub>9</sub>H<sub>9</sub>ClN<sub>4</sub>OS.0.2H<sub>2</sub>O.0.2CH<sub>3</sub>OH) calcd: C 41.43, H 3.85, N 21.01, S 12.02; found: C 41.33, H 3.43, N 20.83, S 11.92.

#### N-(5-Chlorothiazolo[5,4-d]pyrimidin-2-yl)isobutyramide (L4)

Yield 45% (light green solid). mp. 179°C. FTIR  $\nu_{\max}$   $\text{cm}^{-1}$ : 1,686 and 1,583. <sup>1</sup>H-NMR (DMSO-*d*<sub>6</sub>, 400 MHz)  $\delta$ : 1.14 (d, 6H, *J* = 6.8 Hz), 2.81 (m, 1H, *J* = 6.8 Hz), 9.05 (s, 1H), and 12.80 (br, 1H). <sup>13</sup>C-NMR (DMSO-*d*<sub>6</sub>, 100 MHz)  $\delta$ : 19.2, 34.6, 140.3, 149.7, 153.2, 159.0, 165.9, and 177.5. MS (ESI<sup>+</sup>): *m/z*: 257.0 [M+H]<sup>+</sup> and 259.2 [M+2+H]<sup>+</sup>. Anal. (C<sub>9</sub>H<sub>9</sub>ClN<sub>4</sub>OS.0.33H<sub>2</sub>O.0.25CH<sub>3</sub>OH) calcd: C 41.05, H 3.97, N 20.70, S 11.84; found: C 41.10, H 3.95, N 20.83, S 11.42.

#### N-(5-Chlorothiazolo[5,4-d]pyrimidin-2-yl)cyclohexane carboxamide (L5)

Yield 62% (gray solid). mp. 192°C. FTIR  $\nu_{\max}$   $\text{cm}^{-1}$ : 1,694 and 1,579. <sup>1</sup>H-NMR (DMSO-*d*<sub>6</sub>, 400 MHz)  $\delta$ : 1.16–1.87 (m, 10H), 2.56 (tt, 1H, *J*<sub>1</sub> = 3.6 Hz, *J*<sub>2</sub> = 11.2 Hz), 9.05 (s, 1H), and 12.72 (br, 1H). <sup>13</sup>C-NMR (DMSO-*d*<sub>6</sub>, 100 MHz)  $\delta$ : 25.4 (2C), 25.6, 29.0 (2C), 44.0, 140.3, 149.8, 153.2, 159.0, 165.9, and 176.5. MS (ESI<sup>+</sup>): *m/z*: 297.0 [M+H]<sup>+</sup> and 299.1 [M+2+H]<sup>+</sup>. Anal. (C<sub>12</sub>H<sub>13</sub>ClN<sub>4</sub>OS.0.5H<sub>2</sub>O.0.33CH<sub>3</sub>OH) calcd: C 46.66, H 5.01, N 17.41, S 9.96; found: C 46.43, H 4.63, N 17.22, S 9.90.

#### N-(5-Chlorothiazolo[5,4-d]pyrimidin-2-yl)benzamide (L6)

Yield 75% (yellow solid). mp. 229°C. FTIR  $\nu_{\max}$   $\text{cm}^{-1}$ : 1,671 and 1,577. <sup>1</sup>H-NMR (CDCl<sub>3</sub>, 400 MHz)  $\delta$ : 7.55 (t, 2H, *J* = 8.0 Hz), 7.68 (t, 1H,

*J* = 8.0 Hz), 8.01 (d, 2H, *J* = 8.0 Hz), 8.60 (s, 1H), and 10.69 (br, 1H). <sup>13</sup>C-NMR (CDCl<sub>3</sub>, 100 MHz)  $\delta$ : 127.8 (2C), 129.4 (2C), 130.9, 134.0, 139.3, 149.2, 154.8, 159.5, 165.5, and 165.9. MS (ESI<sup>+</sup>): *m/z*: 290.9 [M+H]<sup>+</sup> and 292.9 [M+2+H]<sup>+</sup>. Anal. (C<sub>12</sub>H<sub>7</sub>ClN<sub>4</sub>OS.0.5H<sub>2</sub>O.0.1C<sub>6</sub>H<sub>14</sub>) calcd: C 49.08, H 3.07, N 18.17, S 10.40; found: 48.93, H 2.97, N 17.94, S 10.33.

#### N-(5-Chlorothiazolo[5,4-d]pyrimidin-2-yl)-2-methyl benzamide (L7)

Yield 77% (yellow solid). mp. 172°C. FTIR  $\nu_{\max}$   $\text{cm}^{-1}$ : 1,676 and 1,575. <sup>1</sup>H-NMR (DMSO-*d*<sub>6</sub>, 400 MHz)  $\delta$ : 2.41 (s, 3H), 7.32–7.36 (m, 2H), 7.48 (d, 1H, *J* = 7.6 Hz), 7.64 (d, 1H, *J* = 7.6 Hz), 9.13 (s, 1H), and 13.21 (br, 1H). <sup>13</sup>C-NMR (DMSO-*d*<sub>6</sub>, 100 MHz)  $\delta$ : 20.1, 126.2, 128.9, 131.5, 131.9, 133.2, 137.3, 140.3, 150.1, 153.5, 159.2, 165.9, and 169.3. MS (ESI<sup>+</sup>): *m/z*: 305.0 [M+H]<sup>+</sup> and 307.0 [M+2+H]<sup>+</sup>. Anal. (C<sub>13</sub>H<sub>9</sub>ClN<sub>4</sub>OS.0.2C<sub>2</sub>H<sub>5</sub>OH) calcd: C 51.26, H 3.27, N 17.84, S 10.21; found: 50.95, H 3.51, N 17.49, S 10.35.

#### N-(5-Chlorothiazolo[5,4-d]pyrimidin-2-yl)-2-methoxybenzamide (L8)

Yield 52% (yellow solid). mp. 220°C (decomposition). FTIR  $\nu_{\max}$   $\text{cm}^{-1}$ : 1,673 and 1,575. <sup>1</sup>H-NMR (DMSO-*d*<sub>6</sub>, 400 MHz)  $\delta$ : 3.90 (s, 3H), 7.02–7.22 (m, 2H), 7.56–7.73 (m, 2H), 9.11 (s, 1H), and 11.33 (br, 1H). <sup>13</sup>C-NMR: n.d. MS (ESI<sup>+</sup>): *m/z*: 321.0 [M+H]<sup>+</sup> and 323.1 [M+2+H]<sup>+</sup>. Anal. (C<sub>13</sub>H<sub>9</sub>ClN<sub>4</sub>O<sub>2</sub>S.0.1H<sub>2</sub>O.0.2C<sub>4</sub>H<sub>8</sub>O<sub>2</sub>) calcd: C 48.73, H 3.20, N 16.47, S 9.42; found: C 48.63, H 3.51, N 16.12, S 9.13.

#### 2-Chloro-N-(5-chlorothiazolo[5,4-d]pyrimidin-2-yl)benzamide (L9)

Yield 77% (yellow solid). mp. 188°C (decomposition). FTIR  $\nu_{\max}$   $\text{cm}^{-1}$ : 1,678 and 1,579. <sup>1</sup>H-NMR (CDCl<sub>3</sub>, 400 MHz)  $\delta$ : 7.45–7.50 (m, 2H), 7.53–7.57 (m, 1H), 7.95 (dd, 1H, *J*<sub>1</sub> = 2.0 Hz, *J*<sub>2</sub> = 7.4 Hz), 8.65 (s, 1H), and 10.56 (br, 1H). <sup>13</sup>C-NMR (CDCl<sub>3</sub>, 100 MHz)  $\delta$ : 127.8, 131.0, 131.4, 131.4, 133.8, 139.2, 145.7, 149.2, 154.8, 158.8, 164.5, and 165.8. MS (ESI<sup>+</sup>): *m/z*: 325.00 [M+H]<sup>+</sup>, 327.0 [M+2+H]<sup>+</sup>, and 329.0 [M+4+H]<sup>+</sup>. Anal. (C<sub>12</sub>H<sub>6</sub>Cl<sub>2</sub>N<sub>4</sub>OS.0.5C<sub>4</sub>H<sub>8</sub>O<sub>2</sub>) calcd: C 45.54, H 2.73, N 15.17, S 8.68; found: C 45.73, H 2.37, N 15.52, S 9.01.

#### N-(5-Chlorothiazolo[5,4-d]pyrimidin-2-yl)-2-fluorobenzamide (L10)

Yield 47% (yellow solid). mp. 218°C. FTIR  $\nu_{\max}$   $\text{cm}^{-1}$ : 1,667 and 1,576. <sup>1</sup>H-NMR (DMSO-*d*<sub>6</sub>, 400 MHz)  $\delta$ : 7.36–7.42 (m, 2H), 7.65–7.71 (m, 1H), 7.80 (d, 1H, *J* = 7.2 Hz), 9.13 (s, 1H), and 10.35 (br, 1H). <sup>13</sup>C-NMR (DMSO-*d*<sub>6</sub>, 100 MHz)  $\delta$ : 117.1, 121.7, 125.2, 130.9, 135.0, 140.3, 150.3, 153.6, 158.9, 161.2, 164.8, and 165.8. MS (ESI<sup>+</sup>): *m/z*: 309.1 [M+H]<sup>+</sup> and 311.1 [M+2+H]<sup>+</sup>. Anal. (C<sub>12</sub>H<sub>6</sub>ClFN<sub>4</sub>OS.0.33H<sub>2</sub>O.0.33CH<sub>3</sub>OH) calcd: C 45.54, H 2.47, N 17.23, S 9.81; found: C 45.85, H 2.09, N 17.68, S 9.86.

#### 2-Bromo-N-(5-chlorothiazolo[5,4-d]pyrimidin-2-yl)benzamide (L11)

Yield 65% (dark beige solid). mp. 216 °C. FTIR  $\nu_{\max}$   $\text{cm}^{-1}$ : 1,698 and 1,581. <sup>1</sup>H-NMR (DMSO-*d*<sub>6</sub>, 400 MHz)  $\delta$ : 7.47–7.56 (m, 2H), 7.69 (dd, 1H, *J*<sub>1</sub> = 2.0 Hz, *J*<sub>2</sub> = 7.2 Hz), 7.77 (dd, 1H, *J*<sub>1</sub> = 1.2 Hz, *J*<sub>2</sub> = 7.4 Hz), 9.11 (s, 1H), and 13.46 (br, 1H). <sup>13</sup>C-NMR (DMSO-*d*<sub>6</sub>, 100 MHz)  $\delta$ : 119.6, 128.3, 130.0, 133.0, 133.5, 136.0, 140.3, 150.4, 153.6, 158.7, 165.8, and 167.7. MS (ESI<sup>+</sup>): *m/z*: 368.8 [M+H]<sup>+</sup>, 370.9 [M+2+H]<sup>+</sup>, and 372.9

[M+4H]<sup>+</sup>. Anal. (C<sub>12</sub>H<sub>6</sub>BrClN<sub>4</sub>O<sub>5</sub>) calcd: C 38.99, H 1.64, N 15.16, S 8.68; found: C 39.14, H 1.99, N 15.45, S 8.46.

*N*-(5-Chlorothiazolo[5,4-d]pyrimidin-2-yl)-2-iodobenzamide (L12)

Yield 80% (yellow solid). mp. 216°C. FTIR  $\nu_{\max}$  cm<sup>-1</sup>: 1,690 and 1,579. <sup>1</sup>H-NMR (DMSO-*d*<sub>6</sub>, 400 MHz)  $\delta$ : 7.30 (td, 1H, *J*<sub>1</sub> = 2.0 Hz, *J*<sub>2</sub> = 7.6 Hz), 7.54 (td, 1H, *J*<sub>1</sub> = 1.2 Hz, *J*<sub>2</sub> = 7.6 Hz), 7.62 (dd, 1H, *J*<sub>1</sub> = 1.6 Hz, *J*<sub>2</sub> = 7.6 Hz), 7.98 (dd, 1H, *J*<sub>1</sub> = 0.8 Hz, *J*<sub>2</sub> = 8.0 Hz), 9.15 (s, 1H), and 13.40 (br, 1H). <sup>13</sup>C-NMR (DMSO-*d*<sub>6</sub>, 100 MHz)  $\delta$ : 94.0, 128.6, 129.3, 132.63, 139.8, 139.9, 140.4, 150.4, 153.6, 158.8, 165.8, 169.3. MS (ESI<sup>+</sup>): *m/z*: 416.8 [M+H]<sup>+</sup> and 418.9 [M+2H]<sup>+</sup>. Anal. (C<sub>12</sub>H<sub>6</sub>ClIN<sub>4</sub>O<sub>5</sub>·0.25H<sub>2</sub>O·0.2CH<sub>3</sub>OH) calcd: C 34.27, H 1.72, N 13.10, S 7.49; found: C 34.64, H 2.16, N 12.69, S 7.93.

*N*-(5-Chlorothiazolo[5,4-d]pyrimidin-2-yl)-2-trifluoromethyl benzamide (L13)

Yield 59% (yellow solid). mp. 195°C. FTIR  $\nu_{\max}$  cm<sup>-1</sup>: 1,693 and 1,579. <sup>1</sup>H-NMR (DMSO-*d*<sub>6</sub>, 400 MHz)  $\delta$ : 7.78–7.82 (m, 1H), 7.84–7.87 (m, 2H), 7.91 (d, 1H, *J* = 7.6 Hz), 9.15 (s, 1H), 13.57 (br, 1H). <sup>13</sup>C-NMR (DMSO-*d*<sub>6</sub>, 100 MHz)  $\delta$ : 127.1, 127.1, 129.6 (2C), 131.9, 133.2, 140.3, 150.5 (2C), 153.7, 158.7, 165.8, 167.6. MS (ESI<sup>+</sup>): *m/z*: 359.00 [M+H]<sup>+</sup> and 361.00 [M+2H]<sup>+</sup>. Anal. (C<sub>13</sub>H<sub>6</sub>ClF<sub>3</sub>N<sub>4</sub>O<sub>5</sub>·1H<sub>2</sub>O·0.25C<sub>2</sub>H<sub>5</sub>OH) calcd: C 41.76, H 2.47, N 14.43, S 8.26; found: C 41.54, H 2.52, N 14.22, S 8.30.

*N*-(5-Chlorothiazolo[5,4-d]pyrimidin-2-yl)-4-methyl benzamide (L14)

Yield 75% (yellow solid). mp. 158°C. FTIR  $\nu_{\max}$  cm<sup>-1</sup>: 1,673 and 1,576. <sup>1</sup>H-NMR (CDCl<sub>3</sub>, 400 MHz)  $\delta$ : 2.46 (s, 3H), 7.35 (d, 2H, *J* = 8.0 Hz), 7.93 (d, 2H, *J* = 8.0 Hz), and 8.69 (s, 1H). <sup>13</sup>C-NMR (DMSO-*d*<sub>6</sub>, 100 MHz)  $\delta$ : 21.6, 129.0 (3C), 129.7 (2C), 140.3, 144.4, 149.7, 153.6, 160.2, 164.7, 165.8. MS (ESI<sup>+</sup>): *m/z*: 304.9 [M+H]<sup>+</sup> and 306.9 [M+2H]<sup>+</sup>. Anal. (C<sub>13</sub>H<sub>9</sub>ClN<sub>4</sub>O<sub>5</sub>·0.1H<sub>2</sub>O·0.33CH<sub>3</sub>OH) calcd: C 50.49, H 3.34, N 17.67, S 10.11; found: C 50.84, H 3.45, N 17.56, S 10.32.

*N*-(5-Chlorothiazolo[5,4-d]pyrimidin-2-yl)-4-methoxybenzamide (L15)

Yield 69% (yellow solid). mp. 245°C. FTIR  $\nu_{\max}$  cm<sup>-1</sup>: 1,660 and 1,583. <sup>1</sup>H-NMR (DMSO-*d*<sub>6</sub>, 400 MHz)  $\delta$ : 3.83 (s, 3H), 7.09 (d, 2H, *J* = 8.0 Hz), 8.13 (d, 2H, *J* = 8.0 Hz), and 9.09 (s, 1H). <sup>13</sup>C-NMR (DMSO-*d*<sub>6</sub>, 100 MHz)  $\delta$ : 56.5, 114.6 (2C), 123.7, 131.2 (2C), 140.4, 149.5, 153.5, 160.0, 164.0, 166.9, and 166.3. MS (ESI<sup>+</sup>): *m/z*: 320.9 [M+H]<sup>+</sup> and 322.9 [M+2H]<sup>+</sup>. Anal. (C<sub>13</sub>H<sub>9</sub>ClN<sub>4</sub>O<sub>5</sub>·0.25H<sub>2</sub>O·0.33CH<sub>3</sub>OH) calcd: C 47.68, H 3.25, N 16.68, S 9.55; found: C 47.53, H 3.68, N 16.58, S 9.52.

4-Chloro-*N*-(5-chlorothiazolo[5,4-d]pyrimidin-2-yl)benzamide (L16)

Yield 64% (yellow solid). mp. 293°C. FTIR  $\nu_{\max}$  cm<sup>-1</sup>: 1,668 and 1,577. <sup>1</sup>H-NMR (DMSO-*d*<sub>6</sub>, 400 MHz)  $\delta$ : 7.61 (d, 2H, *J* = 8.0 Hz), 8.10 (d, 2H, *J* = 8.0 Hz), and 9.07 (s, 1H). <sup>13</sup>C-NMR: n.d. MS (ESI<sup>+</sup>): *m/z*: 324.9 [M+H]<sup>+</sup>, 326.9 [M+2H]<sup>+</sup>, and 328.9 [M+4H]<sup>+</sup>. Anal. (C<sub>12</sub>H<sub>6</sub>Cl<sub>2</sub>N<sub>4</sub>O<sub>5</sub>·0.5H<sub>2</sub>O·0.1C<sub>4</sub>H<sub>8</sub>O<sub>2</sub>) calcd: C 43.42, H 2.29, N 16.34, S 9.35; found: C 43.16, H 2.37, N 16.69, S 9.04.

*N*-(5-Chlorothiazolo[5,4-d]pyrimidin-2-yl)-4-fluorobenzamide (L17)

Yield 64% (dark yellow solid). mp. 272°C. FTIR  $\nu_{\max}$  cm<sup>-1</sup>: 1,669 and 1,577. <sup>1</sup>H-NMR (DMSO-*d*<sub>6</sub>, 400 MHz)  $\delta$ : 7.41 (t, 2H, *J* = 8.8 Hz), 8.21 (dd, 2H, *J*<sub>1</sub> = 3.6 Hz, *J*<sub>2</sub> = 5.2 Hz), 9.12 (s, 1H), 13.37 (br, 1H). <sup>13</sup>C-NMR (DMSO-*d*<sub>6</sub>, 100 MHz)  $\delta$ : 116.2, 116.4, 128.0, 128.1, 132.9, 132.0, 140.3, 150.0, 153.5, 160.0, 165.9, and 166.0. MS (ESI<sup>+</sup>): *m/z*: 309.1 [M+H]<sup>+</sup> and 311.1 [M+2H]<sup>+</sup>. Anal. (C<sub>12</sub>H<sub>6</sub>ClFN<sub>4</sub>O<sub>5</sub>·0.5H<sub>2</sub>O·0.2CH<sub>3</sub>OH) calcd: C 45.21, H 2.43, N 17.29, S 9.89; found: C 45.48, H 2.80, N 17.42, S 10.29.

*N*-(5-Chlorothiazolo[5,4-d]pyrimidin-2-yl)-4-nitrobenzamide (L18)

Yield 53% (yellow solid). mp. 214°C. FTIR  $\nu_{\max}$  cm<sup>-1</sup>: 1,672 and 1,580. <sup>1</sup>H-NMR (CDCl<sub>3</sub>, 400 MHz)  $\delta$ : 8.20 (d, 2H, *J* = 8.0 Hz), 8.39 (d, 2H, *J* = 8.0 Hz), and 8.97 (s, 1H). <sup>13</sup>C-NMR (DMSO-*d*<sub>6</sub>, 100 MHz)  $\delta$ : 123.8 (2C), 130.0 (2C), 136.9, 139.9, 150.0, 150.2, 151.0, 153.7, 159.6, and 166.09. MS (ESI<sup>+</sup>): *m/z*: 335.9 [M+H]<sup>+</sup> and 337.9 [M+2H]<sup>+</sup>. Anal. (C<sub>12</sub>H<sub>6</sub>ClN<sub>4</sub>O<sub>5</sub>·0.25C<sub>2</sub>H<sub>5</sub>OH) calcd: C 43.24, H 2.18, N 20.17, S 9.23; found: C 43.10, H 2.36, N 19.93, S 9.64.

2,4-Dichloro-*N*-(5-chlorothiazolo[5,4-d]pyrimidin-2-yl)-benzamide (L19)

Yield 54% (light brown solid). mp. 217°C. FTIR  $\nu_{\max}$  cm<sup>-1</sup>: 1,696 and 1,582. <sup>1</sup>H-NMR (DMSO-*d*<sub>6</sub>, 400 MHz)  $\delta$ : 7.60 (dt, 1H, *J*<sub>1</sub> = 2.0 Hz, *J*<sub>2</sub> = 8.4 Hz), 7.74–7.81 (m, 2H), 9.11 (s, 1H), and 13.57 (br, 1H). <sup>13</sup>C-NMR (DMSO-*d*<sub>6</sub>, 100 MHz)  $\delta$ : 128.0, 130.0, 131.6, 132.2, 132.6, 137.0, 140.3, 150.4, 153.8, 158.7, 165.9, and 166.0. MS (ESI<sup>+</sup>): *m/z*: 358.9 [M+H]<sup>+</sup>, 360.9 [M+2H]<sup>+</sup>, and 362.9 [M+4H]<sup>+</sup>. Anal. (C<sub>12</sub>H<sub>5</sub>Cl<sub>3</sub>N<sub>4</sub>O<sub>5</sub>·0.33H<sub>2</sub>O·0.66CH<sub>3</sub>OH) calcd: C 39.32, H 2.16, N 14.49, S 8.29; found: C 39.72, H 2.23, N 14.46, S 8.03.

*N*-(5-Chlorothiazolo[5,4-d]pyrimidin-2-yl)-3-phenyl propionamide (L20)

Yield 38% (green solid). mp. 202°C. FTIR  $\nu_{\max}$  cm<sup>-1</sup>: 1,693 and 1,583. <sup>1</sup>H-NMR (DMSO-*d*<sub>6</sub>, 400 MHz)  $\delta$ : 2.85 (t, 2H, *J* = 7.8 Hz), 2.94 (d, 2H, *J* = 8 Hz), 7.17 (td, 1H, *J*<sub>1</sub> = 2.0 Hz, *J*<sub>2</sub> = 6.8 Hz), 7.23–7.29 (m, 4H), 9.03 (s, 1H), and 12.78 (br, 1H). <sup>13</sup>C-NMR (DMSO-*d*<sub>6</sub>, 100 MHz)  $\delta$ : 30.6, 37.2, 126.1, 128.7 (2C), 128.84 (2C), 140.5, 140.8, 150.0, 153.3, 158.5, 166.1, and 173.4. MS (ESI<sup>+</sup>): *m/z*: 319.1 [M+H]<sup>+</sup> and 321.0 [M+2H]<sup>+</sup>. Anal. (C<sub>14</sub>H<sub>11</sub>ClN<sub>4</sub>O<sub>5</sub>·0.5C<sub>4</sub>H<sub>8</sub>O) calcd: C 54.16, H 4.26, N 15.79, S 9.04; found: C 54.55, H 4.02, N 16.01, S 8.89.

(*E*)-*N*-(5-Chlorothiazolo[5,4-d]pyrimidin-2-yl)cinnamamide (L21)

Yield 47% (yellow solid). mp. 204°C. FTIR  $\nu_{\max}$  cm<sup>-1</sup>: 1,694 and 1,584. <sup>1</sup>H-NMR (DMSO-*d*<sub>6</sub>, 400 MHz)  $\delta$ : 6.93 (d, 1H, *J* = 16 Hz), 7.45–7.46 (m, 3H), 7.65 (dd, 1H, *J*<sub>1</sub> = 3.0 Hz, *J*<sub>2</sub> = 7.0 Hz), 7.79 (d, 1H, *J* = 16 Hz), and 9.06 (s, 1H). <sup>13</sup>C-NMR (DMSO-*d*<sub>6</sub>, 100 MHz)  $\delta$ : 119.8, 128.6 (2C), 129.5 (2C), 131.0, 134.7, 140.6, 144.5, 149.5, 153.3, 159.4, 165.6, 166.2. MS (ESI<sup>+</sup>): *m/z*: 317.1 [M+H]<sup>+</sup> and 319.1 [M+2H]<sup>+</sup>. Anal. (C<sub>14</sub>H<sub>9</sub>ClN<sub>4</sub>O<sub>5</sub>·1H<sub>2</sub>O·0.1C<sub>4</sub>H<sub>8</sub>O) calcd: C 50.57, H 3.48, N 16.38, S 9.37; found: C 50.20, H 3.50, N 16.75, S 9.70.

*N*-(5-Chlorothiazolo[5,4-*d*]pyrimidin-2-yl)furan-2-carboxamide (L22)  
Yield 64% (orange solid). mp. 225°C (decomposition). FTIR  $\nu_{\max}$   $\text{cm}^{-1}$ : 1,675 and 1,583.  $^1\text{H-NMR}$  (DMSO- $d_6$ , 400 MHz)  $\delta$ : 6.77 (q, 1H,  $J = 1.6$  Hz), 7.77 (dd, 1H,  $J_1 = 0.8$  Hz,  $J_2 = 3.6$  Hz), 8.07 (dd, 1H,  $J_1 = 0.8$  Hz,  $J_2 = 1.8$  Hz), 9.10 (s, 1H), and 13.36 (br, 1H).  $^{13}\text{C-NMR}$  (DMSO- $d_6$ , 100 MHz)  $\delta$ : 112.6, 118.9, 140.2, 145.4, 148.5, 149.7, 153.8, 157.3, 159.2, and 166.4. MS (ESI $^+$ ):  $m/z$ : 281.0 [M+H] $^+$  and 283.1 [M+2+H] $^+$ . Anal. (C $_{10}$ H $_5$ ClN $_4$ O $_2$ S $_0.5$ H $_2$ O) calcd: C 41.46, H 2.09, N 19.34, S 11.07; found: C 41.80, H 2.35, N 19.49, S 11.33.

*N*-(5-Chlorothiazolo[5,4-*d*]pyrimidin-2-yl)thiophene-2-carboxamide (L23)

Yield 49% (yellow solid). mp. 253°C. FTIR  $\nu_{\max}$   $\text{cm}^{-1}$ : 1,694 and 1,584.  $^1\text{H-NMR}$  (DMSO- $d_6$ , 400 MHz)  $\delta$ : 7.27 (t, 1H,  $J_1 = 4.8$  Hz,  $J_2 = 4.0$  Hz), 8.04 (d, 1H,  $J = 4.8$  Hz), 8.32 (d, 1H,  $J = 4.0$  Hz), 9.09 (s, 1H), and 13.36 (br, 1H).  $^{13}\text{C-NMR}$  (DMSO- $d_6$ , 100 MHz)  $\delta$ : 128.7, 133.3, 135.2, 136.9, 140.2, 150.0, 153.7, 159.9, 161.2, and 165.5. MS (ESI $^+$ ):  $m/z$ : 296.9 [M+H] $^+$  and 298.9 [M+2+H] $^+$ . Anal. (C $_{10}$ H $_7$ ClN $_4$ O $_2$ S $_2$ ·0.4H $_2$ O·0.1C $_2$ H $_5$ OH) calcd: C 39.70, H 2.09, N 18.16, S 20.78; found: C 39.62, H 2.52, N 18.49, S 20.36.

## 4.2 | Biological activities

### 4.2.1 | Preparation and purification of recombinant PTR1 enzyme

The *E. coli* expression plasmid carrying the *LmPTR1* gene cloned with the T7 promoter—pET15b-*LmPTR1*—was kindly provided by Prof. W. N. Hunter's (University of Dundee, UK) laboratory. This plasmid was transformed into the chemically competent *E. coli* BL21 strain by heat shock. After transformation, a single colony was selected in Luria-Bertani (LB) agar plates containing 100  $\mu\text{g/ml}$  ampicillin. The selected colony was amplified by incubation at 37°C in 5 ml LB liquid medium containing 50  $\mu\text{g/ml}$  ampicillin for 4 hr, and it was then transferred to 50 ml LB liquid (50  $\mu\text{g/ml}$  ampicillin) medium to increase the volume and incubated until the optical density value reached 0.5–0.6. To obtain a cell pellet, the medium was centrifuged at 10,000 g for 2 min at 4°C. The supernatant was discarded and the pellet was transferred to 250 ml LB liquid medium containing 1 mM of isopropyl  $\beta$ -D-1-thiogalactopyranoside. Incubation was done at 27°C for 16 hr with shaking at 150 rpm.

Cells were harvested after incubation by centrifugation (2,500g) at 4°C. The cell lysate was prepared using following procedures: incubation with 1 mg/ml lysozyme for 30 min at 4°C with shaking; sonication 10 times for 15-s burst–15-s cooling cycles; incubation with 5  $\mu\text{g/ml}$  DNase for 15 min at 4°C; and centrifugation of the lysate at 10,000 g for 30 min at 4°C. Then, the supernatant was transferred to a new Falcon tube. The supernatant was filtered through a 0.45- $\mu\text{m}$  filter to eliminate the particles. Five microliters of supernatant were then applied to an equilibrated affinity chromatography purification column (GE-Protino Ni-TED 2000). The pET15b-*LmPTR1* plasmid codes for a hexa-histidine tag on the

N-terminus of the *LmPTR1* enzyme and allows the use of metal chelate affinity chromatography for the purification. The unbound proteins were washed from the column with a washing buffer. The His-tagged protein was eluted using elution buffer. The removal of the histidine tag was not found necessary for activity due to the disadvantages of the second purification step. The sodium dodecyl sulfate polyacrylamide gel electrophoresis analysis was performed to analyze the purity and molecular weight of the isolated enzyme.

Plasmid DNA isolation was carried out using the Invitrogen MiniPrep pDNA isolation kit. HindIII and EcoRV restriction enzymes were applied to confirm the transformation of pET15b-*LmPTR1*.

### 4.2.2 | In vitro evaluation of *LmPTR1* enzyme inhibition studies

The inhibitory activity of the recombinant *LmPTR1* enzyme was determined by measuring the absorbance at 340 nm in a 96-well plate with a Varioskan Flash multimode reader (Thermo Fisher Scientific). Before the reaction, the enzyme concentration was determined by a bicinchoninic assay (QuantiPro BCA Assay Kit, Sigma-Aldrich). Then, the reaction was carried out at 30°C in the presence of recombinant *LmPTR1* (5  $\mu\text{M}$ ), NADPH (100  $\mu\text{M}$ ), folic acid (30  $\mu\text{M}$ ), and dithiothreitol (5 mM) in a sodium phosphate buffer (pH 6.0).<sup>[21,37]</sup> Folic acid was added to the reaction as the substrate of the *LmPTR1* enzyme, and the reaction was initiated by the addition of freshly prepared NADPH. The total volume of each reaction was 300  $\mu\text{l}$ . The IC $_{50}$  values were calculated by the addition of testing compounds in increasing concentrations (6.25, 12.5, 25, 50, and 100  $\mu\text{M}$ ) in DMSO. The final concentration of DMSO was kept below 1% to avoid an impact on enzyme activity. MTX (Cayman Chemicals) was used at the same concentration range as a positive control. Isolation and purification of the *LmPTR1* enzyme were carried out from a single stock at the beginning of each experiment. The purified enzyme was kept at 4°C and it was not used for longer than 3 days. Experiments were carried out at least in triplicate. The IC $_{50}$  concentration of each compound was calculated by using GraphPad Prism 6.0.

### 4.2.3 | In vitro antileishmanial activity

In vitro antileishmanial activity of the compounds was tested against *L. tropica* (MHOM/AZ/1974/SAF-K27), *L. major* (MHOM/SU/1973/5ASKH), and *L. infantum* (MHOM/TN/1980/IPT1) promastigotes. Promastigotes were grown in Rosewell Park Memorial Institute (RPMI)-1640 medium (Biochrom AG), supplemented with 10% fetal calf serum. The parasites were incubated at 26°C and passaged until log phase (10 $^8$  promastigotes/ml). After centrifuging the parasites for 10 min at 1,500 rpm, they were washed with saline twice. Promastigotes were cultured in 96-well plates (10 $^6$  parasites/well) with or without the compounds. For in vitro experiments, 300, 150, 75, 37.5, 18.8, 9.4, 4.7, and 2.3- $\mu\text{M}$  concentrations of the compounds were prepared in DMSO. As reference drugs, glucantime and AmpB were

prepared in DMSO at the same concentrations of the compounds. The highest concentration of DMSO and RPMI medium was also used for control groups. Microplates were incubated at 25°C. The number of parasites was counted with a hemocytometer under a light microscope after 24, 48, and 72 hr. All the in vitro experiments were run in triplicate and the results were expressed as the percent inhibition in the parasite number. The percentage of viable parasites (viability %) was calculated using the following equation: viability % = (mean of treated live parasites – blank/mean of untreated (control) parasites – blank) × 100.<sup>[38–42]</sup>

J774.2 mouse macrophages were obtained from Parasite Bank located in Manisa Celal Bayar University Faculty of Medicine, Turkey, for amastigote assay. Macrophages were grown in RPMI-1640 medium, supplemented with 15% inactivated fetal bovine serum. Cells were seeded at a density of  $1 \times 10^4$  cells/well in eight-well microplates with rounded coverslips on the bottom, and they were cultured in a humidified 95% air and 5% CO<sub>2</sub> atmosphere at 37°C for 24 hr. Afterward, the cells were infected with in vitro promastigote forms of *L. tropica* in the stationary phase, at a ratio of 10:1, for 24 hr (Figure S15). The nonphagocytosed parasites were removed by washing, and then **L16** and **L19** (300, 150, 75, 37.5, 18.75, 9.37, 4.68, and 2.34 μM) were added. AmpB was used as positive control in 1, 0.5, 0.25, 0.13, 0.06, 0.03, 0.02, and 0.01-μM concentrations. Macrophages were incubated with the compounds for 24 hr at 37°C in 5% CO<sub>2</sub>. After incubation, plates were washed and treated with methanol. Determined preparations were Giemsa-stained and microscopically examined. The number of cellular amastigotes was determined by analyzing 200 host cells distributed in randomly chosen microscopic fields.<sup>[43]</sup>

#### 4.2.4 | Cytotoxicity

The cytotoxicity evaluation of selected compounds was performed on RAW264.7 murine macrophage cell line (ATCC® TIB-71™). Cells were cultured in a Dulbecco's modified Eagle's medium, supplemented with 2-mM L-glutamine and 10% fetal bovine serum. Bacterial contamination was prevented by the addition of penicillin–streptomycin (100 UI/ml penicillin, 100 μg/ml streptomycin). For cytotoxicity assay, the cells were seeded in 96-well culture plates at a density of  $10^5$  cells/ml. After overnight incubation, the medium was removed and cells were washed with Dulbecco's phosphate-buffered saline (DPBS). One hundred microliters of fresh growth medium including increasing concentrations of synthesized compounds were immediately added after the washing step. The following concentrations of samples were added into the wells: 6.25, 12.5, 25, 50, and 100 μM/well. Control groups and blind groups for spectroscopic analysis were also applied.

The viability of cells was determined by the colorimetric WST-1 cell proliferation assay kit as per the manufacturer's instructions (Roche). Briefly, after overnight incubation, the growth medium containing the samples was removed and cells were washed with DPBS. Then, 100-μl fresh growth medium and 10-μl WST-1 reagent

were added to each well and incubated for 2.5 hr at 37°C. Viable cells enzymatically convert the colorless tetrazolium salt to an orange-colored formazan compound. The intensity of the formed color was measured spectrophotometrically at 475 nm in a Varioskan Flash multimode reader (Thermo Fisher Scientific). Blank samples were used to subtract background absorption. To eliminate nonspecific absorbance occurrences from the medium, the absorbance at 660 nm was also measured. Specific absorbance values were expressed mathematically with the following equation: Specific absorbance =  $A_{475 \text{ nm}}(\text{test}) - A_{475 \text{ nm}}(\text{blank}) - A_{660 \text{ nm}}(\text{test})$ .

Cell viability was calculated on the basis of the specific absorbance of the cells, compared with the absorbance of the control group consisting of untreated RAW264.7 cells. IC<sub>50</sub> values were calculated according to the cell viability values using the Prism 6.0 (GraphPad) software. Experiments were carried out at least in triplicate.

### 4.3 | Molecular modeling studies

The studied compounds were generated with a builder panel of MOE2016.08, protonated using the protonate three-dimensional protocol, and subjected to energy minimization with MOE2016.08 using the MMFF94x force field.<sup>[44,45]</sup> The crystal structure of pteridine reductase 1 (PDB id: 2BFA resolved at 2.7 Å) was taken from the RCSB Protein Data Bank (<http://www.rcsb.org/pdb>). Chain A and NADPH of the crystal structure were selected to prepare docking structure and chain B; heteroatoms and water molecules in the PDB file were deleted. Antechamber and parmchk modules of AmberTools 16 were used to calculate the partial atomic charges for NADPH with the AM1-BCC charge model and generate the parameter files of NADPH, respectively.<sup>[46,47]</sup> The complex of chain A and NADPH was prepared using the xleap module of AmberTools 16 with the General Amber force field (GAFF) for NADPH and AMBER99SB force field for protein, and it was solvated in an octahedral box with TIP3P water molecules with 10 Å distance between the protein surface and the box boundary.<sup>[48]</sup> The solvated system was neutralized with an appropriate number of chloride counter ions and subjected to energy minimization with Sander.MPI module of Amber 12 suite. Before the docking study, created chloride counterions and water molecules (excluded the water molecules included in the binding site) were removed from the system.

A docking study was performed using the GOLD 5.2.1 program with default generic algorithm parameters. The studied compounds were docked within a radius of 20 Å around the oxygen atom (O) of the carbonyl group of Gly225 residue. In total, 100 conformations were allowed per structure. The GoldScore fitness function was used as scoring functions.<sup>[49,50]</sup> Figures were created with the MOE2016.08 program.

Molecular dynamics simulations were carried out for NADPH–protein (*LmPTR1*) and ligand–NADPH–protein complexes using AMBER 12 suite.<sup>[46]</sup> The initial ligand–NADPH–protein systems were generated using the first solution of compounds **L1**, **L9**, **L16**, and

L18 in LmPTR1 yielded from docking studies. The partial atomic charges for the title compounds and NADP were calculated with antechamber module of AmberTools 16 using the AM1-BCC charge model.<sup>[46,47]</sup> The Xleap module of AmberTools 16 was used to parameterize the complexes using general AMBER force field (gaff) for ligands and NADP and AMBERff99SB force field for proteins, to solvate the complexes in an octahedral box with TIP3P water molecules with 10 Å distance between the protein surface and the box boundary, and to neutralize the solvated systems with an appropriate number of chlorine counter ions.<sup>[46,48,51,52]</sup> The energy minimizations and MD simulations of the systems were executed with SANDER.MPI and PMEMD.CUDA modules of AMBER 12, respectively.<sup>[47]</sup> The initial systems were exposed to energy minimization in two steps: restraining initial structures for 1,000 iterations with the steepest descent algorithm and for 1,000 iterations with conjugate gradient methods, and then minimizing entire systems for 2,500 iterations using steepest descent algorithm and for 2,500 iterations using conjugate gradient methods. The systems were heated from 0 to 300 K, with 10-kcal-mol<sup>-1</sup>·Å<sup>-1</sup> restraint force permitting water molecules and ions to move freely for 0.1 ns, and the temperature was equilibrated at 300 K with a collision frequency of 1.0 ps<sup>-1</sup> in constant volume periodic boundary and pressure at 1 bar. The positional restraints were kept for the solute using constant pressure periodic boundary conditions with isotropic position scaling method using Langevin dynamics for 2 ns in the MD simulations. The positional constraints were gradually removed, keeping the temperature at 300 K and pressure at 1 bar, and the systems were subjected to free MD simulation for 100 ns. The SHAKE algorithm was performed to constrain bond vibrations involving hydrogen atoms in the equilibration part of MD and the free MD simulations.<sup>[53]</sup> The Particle Mesh Ewald method was executed for long-range electrostatic interactions using 10-Å cutoff for the short-range nonbonded interactions and 2 fs for a time step.<sup>[54]</sup> Xmgrace program was used for visualization of the trajectories.<sup>[55]</sup> The hydrogen bonding was determined with Cpptraj module of AmberTools 16 using default parameters.<sup>[56]</sup> Binding free energies of compounds were calculated with MMPBSA.py.MPI module of AmberTools 16 using the Generalized Born (GB) model from 100 spaced snapshots of the last 40 ns of the unrestrained MD simulations.<sup>[57]</sup> MD snapshots were taken out from free MD simulations using the UCSF Chimera package.<sup>[58]</sup> Figures were set up with the MOE2016.08 program.

## ACKNOWLEDGMENTS

We would like to thank Prof. W. N. Hunter (University of Dundee, UK) for the LmPTR1 construct and Pharmaceutical Sciences Research Centre (FABAL) at Ege University Faculty of Pharmacy for spectral analyses of the compounds and Molecular Modeling Software support, and Parasite Bank of Medical School of Manisa Celal Bayar University for all support. The authors extend their appreciation to the Scientific and Technological Research Council of Turkey (TUBITAK), project no. SBAG-213-S-026 and Ege University Science and Technology Centre (EBILTEM), grant no. 2014BIL003.

## CONFLICT OF INTERESTS

The authors declare that there are no conflict of interests.

## ORCID

Huseyin Istanbulu  <http://orcid.org/0000-0002-0102-4181>

Gulsah Bayraktar  <http://orcid.org/0000-0001-7271-1619>

Hasan Akbaba  <http://orcid.org/0000-0001-9273-6346>

Gunes Coban  <http://orcid.org/0000-0003-4512-4392>

Bilge Debelec Butuner  <http://orcid.org/0000-0001-8112-9241>

Ahmet Ozbilgin  <http://orcid.org/0000-0003-3613-8741>

Vildan Alptuzun  <http://orcid.org/0000-0002-1477-4440>

## REFERENCES

- [1] WHO Leishmaniasis Fact Sheet, Updated March 2019. <https://www.who.int/en/news-room/fact-sheets/detail/leishmaniasis> (accessed: October 2019)
- [2] DNDi Leishmaniasis Fact Sheet, [https://www.dndi.org/wp-content/uploads/2019/09/Factsheet2019\\_Leishmaniasis.pdf](https://www.dndi.org/wp-content/uploads/2019/09/Factsheet2019_Leishmaniasis.pdf) (accessed: October 2019)
- [3] P. Pottinger, C. R. Sterling *Sherris Medical Microbiology*, 6th ed. (Eds: K. C. Ryan, C. G. Ray), McGraw-Hill Education, New York 2014, pp. 823–845.
- [4] A. Özbilgin, G. Çulha, S. Uzun, M. Harman, S. G. Topal, F. Okudan, F. Zeyrek, C. Gündüz, İ. Östan, M. Karakuş, S. Töz, Ö. Kurt, I. Akyar, A. Erat, D. Güngör, Ç. Kayabaşı, İ. Çavuş, P. Bastien, F. Pratlong, T. Kocagöz, Y. Özbel, *Trop. Med. Int. Health* 2016, 21, 783.
- [5] W. L. Roberts, W. J. McMurray, P. M. Rainey, *Antimicrob. Agents Chemother.* 1998, 42, 1076.
- [6] H. R. Hansen, C. Hansen, K. P. Jensen, S. H. Hansen, S. Sturup, B. Gammelgaard, *Anal. Chem.* 2008, 80, 5993.
- [7] WHO Technical Report, Series 949, Control of the Leishmaniasis: Report of a meeting of the WHO Expert Committee on the Control of Leishmaniasis, Geneva, Switzerland 2010.
- [8] S. L. Croft, S. Sundar, A. H. Fairlamb, *Clin. Microbiol. Rev.* 2006, 19, 111.
- [9] S. Sundar, A. Singh, M. Rai, V. K. Prajapati, A. K. Singh, B. Ostyn, M. Boelaert, J. C. Dujardin, J. Chakravarty, *Clin. Infect. Dis.* 2012, 55, 543.
- [10] O. P. Singh, B. Singh, J. Chakravarty, S. Sundar, *Infect. Dis. Poverty* 2016, 5, 19.
- [11] A. Alawieh, U. Musharrafieh, A. Jaber, A. Berry, N. Ghosn, A. R. Bizri, *Int. J. Infect. Dis.* 2014, 29, 115.
- [12] N. Salam, W. M. Al-Shaqha, A. Azzi, *PLOS Negl. Trop. Dis.* 2014, 8, e3208.
- [13] A. R. Bello, B. Nare, D. Freedman, L. Hardy, S. Beverley, *Proc. Natl. Acad. Sci. U. S. A.* 1994, 91, 11442.
- [14] B. Nare, L. W. Hardy, S. M. Beverley, *J. Biol. Chem.* 1997, 272, 13883.
- [15] T. J. Vickers, S. M. Beverley, *Essays Biochem.* 2011, 51, 63.
- [16] H. L. Callahan, S. M. Beverley, *J. Biol. Chem.* 1992, 267, 24165.
- [17] B. Papadopoulou, G. Roy, M. Ouellette, *EMBO J.* 1992, 11, 3601.
- [18] D. G. Gourley, A. W. Schüttelkopf, G. A. Leonard, J. Luba, L. W. Hardy, S. M. Beverley, W. N. Hunter, *Nat. Struct. Biol.* 2001, 8, 521.
- [19] K. McLuskey, F. Gibellini, P. Carvalho, M. A. Averyc, W. N. Hunter, *Acta Crystallogr. Sect. D: Biol.* 2004, D60, 1780.
- [20] J. Drummelsmith, V. Brochu, I. Girard, N. Messier, M. Ouellette, *Mol. Cell. Proteomics* 2003, 2, 146.
- [21] A. Cavazzuti, G. Paglietti, W. N. Hunter, F. Gamarro, S. Piras, M. Loriga, S. Allecca, P. Corona, K. McLuskey, L. Tulloch, F. Gibellini, S. Ferrari, M. P. Costi, *Proc. Natl. Acad. Sci. U. S. A.* 2008, 105, 1448.
- [22] K. S. van Horn, X. Zhu, T. Pandharkar, S. Yang, B. Vesely, M. Vanaerschot, J. C. Dujardin, S. Rijal, D. E. Kyle, M. Z. Wang, K. A. Werbovetz, R. Manetsch, *J. Med. Chem.* 2014, 57, 5141.

- [23] C. Mendoza-Martínez, J. Correa-Basurto, R. Nieto-Meneses, A. Márquez-Navarro, R. Aguilar-Suárez, M. D. Montero-Cortés, B. Noguera-Torres, E. Suárez-Contreras, N. Galindo-Sevilla, Á. Rojas-Rojas, A. Rodríguez-Lezama, F. Hernández-Luis, *Eur. J. Med. Chem.* **2015**, *96*, 296.
- [24] A. H. Romero, N. Rodríguez, H. Oviedo, *Bioorg. Chem.* **2019**, *83*, 145.
- [25] S. Ferrari, F. Morandi, D. Motiejunas, E. Nerini, S. Henrich, R. Luciani, A. Venturelli, S. Lazzari, S. Calò, S. Gupta, V. Hannaert, P. Michels, R. C. Wade, M. P. Costi, *J. Med. Chem.* **2011**, *54*, 211.
- [26] C. P. Mpamhanga, D. Spinks, L. B. Tulloch, E. J. Shanks, D. A. Robinson, I. T. Collie, A. H. Fairlamb, P. G. Wyatt, J. A. Frearson, W. N. Hunter, I. H. Gilbert, R. Brenk, *J. Med. Chem.* **2009**, *52*, 4454.
- [27] A. I. Khalaf, J. K. Huggan, C. J. Suckling, C. L. Gibson, K. Stewart, F. Giordani, M. P. Barrett, P. E. Wong, K. L. Barrack, W. N. Hunter, *J. Med. Chem.* **2014**, *57*, 6479.
- [28] Q. Dong, X. Gong, X. M. Hirose, B. Jin, F. Zhou, WO 2010/008847 A2, **2010**.
- [29] N. Whittaker, *J. Chem. Soc.* **1951**, 1565.
- [30] A. C. Schuemaker, R. W. Hoffmann, *Synthesis* **2001**, *2*, 243.
- [31] H. E. Gottlieb, V. Kotlyar, A. Nudelman, *J. Org. Chem.* **1997**, *62*, 7512.
- [32] G. R. Fulmer, A. J. M. Miller, N. H. Sherden, H. E. Gottlieb, A. Nudelman, B. M. Stoltz, J. E. Bercau, K. I. Goldberg, *Organometallics* **2010**, *29*, 2176.
- [33] B. Nare, J. Luba, L. W. Hardy, S. Beverley, *Parasitology* **1997**, *114*, S101.
- [34] L. Monzote, A. Lackova, K. Staniek, S. Steinbauer, G. Pichler, W. Jäger, L. Gille, *Parasitology* **2017**, *144*, 747.
- [35] A. A. Dar, M. Shadab, S. Khan, N. Ali, A. T. Khan, *J. Org. Chem.* **2016**, *81*, 3149.
- [36] M. Machado, P. Pires, A. M. Dinis, M. Santos-Rosa, V. Alves, L. Salgueiro, C. Cavaleiro, M. C. Sousa, *Exp. Parasitol.* **2012**, *130*, 223.
- [37] L. W. Hardy, W. Matthews, B. Nare, S. M. Beverley, *Exp. Parasitol.* **1997**, *87*, 157.
- [38] I. Ostan, H. Saglam, M. E. Limoncu, H. Ertabaklar, S. O. Toz, Y. Ozbek, A. Ozbilgin, *New Microbiol.* **2007**, *30*, 439.
- [39] A. Ozbilgin, C. Durmuskahya, H. Kayalar, H. Ertabaklar, C. Gunduz, I. Ural, F. Zeyrek, O. Kurt, I. Cavus, S. O. Toz, Y. Ozbek, *Trop. J. Pharm. Res.* **2014**, *13*, 2047.
- [40] E. Polat, H. Cakan, M. Aslan, S. Sirekbasan, Z. Kutlubay, T. Ipek, A. Ozbilgin, *Exp. Parasitol.* **2012**, *132*, 129.
- [41] M. E. Limoncu, B. Erac, T. Gurpinar, A. Ozbilgin, C. Balcioglu, M. Hosgor-Limoncu, *Turkiye. Parazitol. Derg.* **2013**, *37*, 1.
- [42] C. Williams, O. A. Espinosa, H. Montenegro, L. Cubilla, T. L. Capson, E. Ortega-Barria, L. I. Romero, *J. Microbiol. Methods* **2003**, *55*, 813.
- [43] C. Marín, I. Ramírez-Macías, M. J. Rosales, B. Muro, F. Reviriego, P. Navarro, V. J. Arán, M. Sánchez-Moreno, *Acta Trop.* **2015**, *148*, 170.
- [44] Molecular Operating Environment (MOE) Chemical Computing Group Inc., Montreal, Canada **2014**.
- [45] T. A. Halgren, *J. Comput. Chem.* **1996**, *17*, 490.
- [46] D. A. Case, T. A. Darden, T. E. Cheatham, C. L. Simmerling, J. Wang, R. E. Duke, R. Luo, R. C. Walker, W. Zhang, K. M. Merz, B. P. Roberts, S. Hayik, A. Roitberg, G. Seabra, J. Swails, A. W. Götz, I. Kolossváry, K. F. Wong, F. Paesani, J. Vanicek, R. M. Wolf, J. Liu, X. Wu, S. R. Brozell, T. Steinbrecher, H. Gohlke, Q. Cai, X. Ye, J. Wang, M.-J. Hsieh, D. R. Roe, D. H. Mathews, M. G. Seetin, R. Solomon-Ferrer, C. Sagui, V. Babin, T. Luchko, S. Gusarov, A. Kovalenko, P. A. Kollman, *AMBER 12*, University of California, San Francisco, CA **2012**.
- [47] A. Jakalian, B. L. Bush, D. B. Jack, *J. Comput. Chem.* **2000**, *21*, 132.
- [48] W. L. Jorgensen, J. Chandrasekhar, J. D. Madura, *J. Chem. Phys.* **1983**, *79*, 926.
- [49] G. Jones, P. Willett, R. C. Glen, *J. Mol. Biol.* **1995**, *245*, 43.
- [50] G. Jones, P. Willett, R. C. Glen, A. R. Leach, R. Taylor, *J. Mol. Biol.* **1997**, *267*, 727.
- [51] J. Wang, R. M. Wolf, J. W. Caldwell, P. A. Kollman, D. A. Case, *J. Comput. Chem.* **2004**, *25*, 1157.
- [52] V. Hornak, R. Abel, A. Okur, B. Strockbine, A. Roitberg, C. Simmerling, *Proteins: Struct., Funct., Bioinf.* **2006**, *65*, 712.
- [53] J. P. Ryckaert, G. Ciccotti, H. J. C. Berendsen, *J. Comput. Phys.* **1977**, *23*, 327.
- [54] U. Essmann, L. Perera, M. L. Berkowitz, T. Darden, H. Lee, L. G. Pedersen, *J. Chem. Phys.* **1995**, *103*, 8577.
- [55] Grace Development Team, <http://plasma-gate.weizmann.ac.il/Grace/>. Accessed October 5, 2019.
- [56] D. R. Roe, T. E. Cheatham III, *J. Chem. Theory Comput.* **2013**, *9*, 3084.
- [57] B. R. Miller III, T. D. McGee Jr., J. M. Swails, N. Homeyer, H. Gohlke, A. E. Roitberg, *J. Chem. Theory Comput.* **2012**, *8*, 3314.
- [58] E. F. Pettersen, T. D. Goddard, C. C. Huang, G. S. Couch, D. M. Greenblatt, E. C. Meng, T. E. Ferrin, *J. Comput. Chem.* **2004**, *13*, 1605.

## SUPPORTING INFORMATION

Additional supporting information may be found online in the Supporting Information section.

**How to cite this article:** Istanbul H, Bayraktar G, Akbaba H, et al. Design, synthesis, and in vitro biological evaluation of novel thiazolopyrimidine derivatives as antileishmanial compounds. *Arch Pharm.* 2020;e1900325.  
<https://doi.org/10.1002/ardp.201900325>